Assessment of the Tao-Mo nonempirical semilocal density functional in applications to solids and surfaces

Yuxiang Mo, Roberto Car, Viktor N. Staroverov, Gustavo E. Scuseria, and Jianmin Tao

Phys. Rev. B **95**, 035118 — Published 12 January 2017

DOI: 10.1103/PhysRevB.95.035118

Assessment of the Tao-Mo nonempirical semilocal density functional in applications to solids and surfaces

Yuxiang Mo[1,2], Roberto Car[3], Viktor N. Staroverov[4], Gustavo E. Scuseria[5], and Jianmin Tao[1,2,*]

[1]Department of Physics, Temple University, Philadelphia, PA 19122-1801, USA
[2]Department of Chemistry, University of Pennsylvania, Philadelphia, PA 19104-6323, USA
[3]Department of Chemistry, Princeton University, Princeton, NJ 08544, USA
[4]Department of Chemistry, The University of Western Ontario, London, Ontario N6A 5B7, Canada
[5]Department of Chemistry, Rice University, Houston, TX 77005, USA

Abstract

Recently, Tao and Mo developed a new semilocal exchange-correlation density functional. The exchange part of this functional is derived from a density matrix expansion corrected to reproduce the fourth-order gradient expansion in the slowly-varying-density limit, while the correlation part is based on the TPSS correlation functional with a modification for the low-density limit. In the present work, the Tao-Mo functional is assessed by computing various properties of solids and jellium surfaces. This includes 22 lattice constants and bulk moduli, 30 band gaps, 7 cohesive energies, and jellium surface exchange and correlation energies for the density parameter r_s in the range from 2 to 3 bohrs. Our calculations show that the Tao-Mo meta-generalized gradient approximation can yield consistently high accuracy for most properties considered here, with mean absolute errors of 0.025 Å for lattice constants, 7.0 GPa for bulk moduli, 0.08 eV/atom for cohesive energies, and 35 erg/cm^2 for surface exchange-correlation energies. The mean absolute error in band gaps is larger than that of TPSS, but slightly smaller than the errors of LSDA, PBE, and revTPSS. However, band gaps are still underestimated, particularly for large-gap semiconductors, compared to the HSE06 nonlocal screened hybrid functional.

PACS numbers: 71.15.Mb, 71.15.Ap, 61.50.Ah, 62.20.Dc

1. Introduction

The Kohn-Sham density functional theory [1] is the most widely used method for electronic structure calculations of molecules and solids. In this theory, only the exchange-correlation energy component that accounts for all many-body effects must be approximated as a functional of the electron density. Therefore, development of accurate and widely applicable exchange-correlation energy functionals has been a primary goal of this theory.

Although many exact properties of the exchange-correlation functional have been discovered, the exact functional itself remains unknown. Approximations can be constructed by assuming some functional form that contains many parameters under the guidance of some basic properties such as uniform coordinate scaling, spin scaling, negativity of the energy density, uniform-gas limit, and slowly-varying gradient expansion. The parameters introduced, or part of them, can be determined by a fit to experiment or highly accurate theoretical reference values for selected properties and systems. Such functionals are called empirical or semiempirical. Density functionals can also be developed by imposing exact or nearly exact constraints, so that all introduced parameters can be fixed by the imposed constraints. Approximate functionals of this type are called nonempirical. Nonempirical functionals may not be as accurate as empirical functionals for certain properties or sets of properties, but they provide a more balanced description of physically different systems such as molecules, solids, and surfaces, because parameters determined by universal constraints are more easily transferable from one system to another than those determined through empirical fitting. This has been demonstrated by the universally good performance of the nonempirical Perdew-Burke-Ernzerhof [2] (PBE) generalized-gradient approximation (GGA) and Tao-Perdew-Staroverov-Scuseria [3] (TPSS) meta-GGA. On the other hand, empirical functionals can be highly accurate for subsets of systems and properties, pushing semilocal DFT to the accuracy limit for a particular functional form. For example, the M06L functional developed by Zhao and Truhlar [4] contains 38 fitting parameters, but shows high accuracy in quantum chemistry. However, it is

relatively less accurate in condensed-matter physics (e.g., the error of M06-L in lattice constants is greater than those of PBE and TPSS [5]).

Physically, the exchange-correlation energy arises from the interaction between an electron and the exchange-correlation hole surrounding the electron. The exchange-correlation hole associated with a given semilocal functional is generally unknown, but it can be constructed by the reverse-engineering approach. By construction, the hole is constrained to reproduce the exchange-correlation energy of the corresponding energy functional. There are many forms of the associated hole that can satisfy this and other constraints. [6–8] Therefore, additional approximations have to be introduced in the construction of the hole.

In the development of semilocal DFT, an appealing approach is to approximate the exchange-correlation hole directly, from which the energy functional can be obtained. [2,9] Recently, Tao and Mo [10] developed a meta-generalized gradient approximation (meta-GGA) for the exchange-correlation energy. In this work, we assess the performance of the Tao-Mo (TM) meta-GGA on lattice constants, bulk moduli, band gaps, cohesive energies of solids, and surface exchange and correlation energies of jellium. Our numerical tests show that this density functional can achieve high accuracy for a variety of solids and surfaces.

2. Computational Method

The TM functional is a meta-GGA of the form [10]

$$E_{\mathrm{xc}}\left[n_{\uparrow},n_{\downarrow}\right]=\int d^{3}r\; n\epsilon_{\mathrm{xc}}^{\mathrm{unif}}\left(n_{\uparrow},n_{\downarrow}\right)F_{\mathrm{xc}}\left(n_{\uparrow},n_{\downarrow},\nabla n_{\uparrow},\nabla n_{\downarrow},\tau_{\uparrow},\tau_{\downarrow}\right), \tag{1}$$

where $n(\mathbf{r})=n_{\uparrow}(\mathbf{r})+n_{\downarrow}(\mathbf{r})$ is the total electron density, $\epsilon_{\mathrm{xc}}^{\mathrm{unif}}\left(n_{\uparrow},n_{\downarrow}\right)$ is the exchange-correlation energy per electron of a uniform electron gas, F_{xc} is the enhancement factor, and $\tau_{\sigma}(\mathbf{r})=\frac{1}{2}\sum_{i}\left|\nabla\phi_{i\sigma}(\mathbf{r})\right|^{2}$ is the Kohn-Sham kinetic energy density of σ-spin electrons.

For a spin-unpolarized density, the exchange part of the TM meta-GGA enhancement factor consists of two parts: one is derived from a density-matrix expansion (DME)[11] and the other is a slowly-varying-density correction (SC),

$$F_{\mathrm{x}} = wF_{\mathrm{x}}^{\mathrm{DME}} + (1-w)F_{\mathrm{x}}^{\mathrm{SC}}. \tag{2}$$

The DME part is given by

$$F_{\mathrm{x}}^{\mathrm{DME}} = \frac{1}{f^2} + \frac{7}{9f^4}\left\{1 + \frac{595}{54}(2\lambda-1)^2 p - \frac{1}{\tau^{\mathrm{unif}}}\left[\tau - 3\left(\lambda^2 - \lambda + \frac{1}{2}\right)\left(\tau - \tau^{\mathrm{unif}} - \frac{1}{72}\frac{|\nabla n|^2}{n}\right)\right]\right\}, \tag{3}$$

where $\tau^{\mathrm{unif}} = 3k_F^2 n/10$ is the kinetic energy density of a uniform electron gas, $p = s^2 = (|\nabla n|/2k_F n)^2$, $k_F = (3\pi^2 n)^{1/3}$ is the Fermi wave vector, $f = \left[1 + 10(70y/27) + \beta y^2\right]^{1/10}$, $y = (2\lambda-1)^2 p$, with $\lambda = 0.6866$, and $\beta = 79.873$. In the slowly-varying-density limit, the first term on the right-hand side of Eq. (3) reduces to 1, while the second term vanishes. Therefore, the DME recovers the correct uniform-gas limit, but the gradient expansion coefficients are not correct. The required slowly-varying-density correction $F_{\mathrm{x}}^{\mathrm{SC}}$ is given by

$$F_{\mathrm{x}}^{\mathrm{SC}} = \left\{1 + 10\left[\left(\frac{10}{81} + \frac{50}{729}p\right)p + \frac{146}{2025}\tilde{q}^2 - \frac{73}{405}\tilde{q}\frac{3}{5}\left(\frac{\tau_W}{\tau}\right)\left(1 - \frac{\tau_W}{\tau}\right)\right] + 0\cdot p^2\right\}^{1/10}, \tag{4}$$

where $\tilde{q} = 3\tau/2k_F^2 n - 9/20 - p/12$ and $\tau_W = |\nabla n|^2/8n$ is the von Weizsäcker kinetic energy density. In the slowly-varying limit, $F_{\mathrm{x}}^{\mathrm{SC}}$ reduces to the exact fourth-order gradient expansion,[6] while the DME part vanishes as $O(\nabla^6 n)$. The weight is given by

$$w = \frac{(\tau_W/\tau)^2 + 3(\tau_W/\tau)^3}{\left[1+(\tau_W/\tau)^3\right]^2}. \quad (5)$$

For one-electron densities, $w=1$, while in the uniform-gas limit, $w=0$. In the slowly-varying-density limit, our enhancement factor of Eq. (2) correctly reduces to F_x^{SC}.

The correlation part of the TM meta-GGA functional takes the same form as TPSS correlation [Eqs. (11) and (12) of Ref. 3], but replaces $C(\zeta,\xi)$ with a simpler form

$$C(\zeta,\xi) = \frac{0.1\zeta^2 + 0.32\zeta^4}{\left\{1+\xi^2\left[(1+\zeta)^{-4/3}+(1-\zeta)^{-4/3}\right]/2\right\}^4}, \quad (6)$$

where $\zeta = (n_\uparrow - n_\downarrow)/n$ is the relative spin polarization and $\xi = |\nabla\zeta|/2k_F$. This modification is motivated by the fact that, in the low-density limit, correlation shows exchange-like scaling behavior, while in the high-density limit, correlation scales to a constant, indicating the significance of correlation in the low-density limit.[13] (Modification of the TPSS correlation energy functional is equivalent to modification of the TPSS correlation hole, because the latter can be reverse-engineered from the former.[6–8])

3. Results and Discussion

3.1 Lattice Constants

The equilibrium lattice constant of a solid is a basic quantity on which all other properties depend. Accurate prediction of this quantity is critical to the design of materials and devices.[14–16] Our test set of 22 bulk crystals includes main-group metals Li, K, Al, semiconductors diamond, Si, β-SiC, Ge, BP, AlP, AlAs, GaN, GaP, GaAs, ionic crystals NaCl, NaF, LiCl, LiF, MgO, MgS, and transition metals Cu, Pd, Ag. Calculations on these solids were performed using a locally modified version[10] of the Gaussian

program [17] with periodic boundary conditions (PBC). [18] Summarized in Table I are the basis sets used in the calculation of the 22 bulk solids. Gaussian-type basis set developed for atoms and molecules often contain diffuse functions. When applying Gaussian-type basis sets to solid systems, such diffuse functions should be removed for computational efficiency. For smooth convergence and reliability of results, dense *k*-point meshes were used: 22×22×22 to 20×40×40 for main-group metals, 10×10×10 to 12×12×12 for semiconductors, 10×10×10 to 14×14×14 for ionic crystals, and 8×16×16 to 10×18×18 for transition metals.

Table I: The Gaussian-type basis sets adopted for the atoms of the 22 bulk solids. The Strukturbericht symbols in parentheses denote the types of crystal structures: face-centered cubic (A1), body-centered cubic (A2), diamond (A4), rock salt (B1), and zinc blende (B3). The "Cartesian" configuration includes six *d* functions. The ''pure'' configuration includes five *d* functions.

Solid	Basis set		*d* functions
Li (A2)	4*s*,3*p*,1*d* [19]		pure
K (A2)	6*s*,4*p*,1*d* [20]		Cartesian
Al (A1)	6*s*,3*p*,1*d* [21]		Cartesian
C (A4)	6-31G*		Cartesian
Si (A4)	6-31G*		Cartesian
SiC (B3)	Si: 6-31G*	C: 6-31G*	Cartesian
Ge (A4)	ECP-4*s*,3*p*,2*d* [22]		pure
BP (B3)	B: 4*s*,3*p*,1*d* [22]	P: 6*s*,5*p*,1*d* [22]	pure
AlP (B3)	Al: 6*s*,3*p*,1*d* [21]	P: 6-311G*	pure
AlAs (B3)	Al: 6*s*,3*p*,1*d* [21]	As: 6-311G*	pure
GaN (B3)	Ga: 6*s*,5*p*,2*d* [23]	N: 6-311G*	pure
GaP (B3)	Ga: 6*s*,5*p*,2*d* [23]	P: 6-311G*	pure
GaAs (B3)	Ga: 6*s*,5*p*,2*d* [23]	As: 6-311G*	pure
NaCl (B1)	Na: 6*s*,4*p*,1*d* [24]	Cl: 6-311G*	pure
NaF (B1)	Na: 6*s*,4*p*,1*d* [24]	F: 6-311G*	pure
LiCl (B1)	Li: 4*s*,3*p*,1*d* [24]	Cl: 6-311G*	pure
LiF (B1)	Li: 4*s*,3*p*,1*d* [24]	F: 6-311G*	pure
MgO (B1)	Mg: 4*s*,3*p*,1*d* [25]	O: 4*s*,3*p*,1*d* [25]	pure
MgS (B1)	Mg: 4*s*,3*p*,1*d* [25]	S: 6-311G*	pure
Cu (A1)	6*s*,5*p*,2*d* [26]		pure
Pd (A1)	ECP [27]-4*s*,4*p*,2*d* [28]		pure
Ag (A1)	ECP [27]-4*s*,4*p*,2*d* [29]		pure

Listed in Table II are the equilibrium lattice constants of the 22 solids calculated with TM and other DFT methods. Figure 1 compares the errors of LSDA, PBE, TPSS, PBEsol, revTPSS, and TM for lattice constants of these solids. The TM functional has a mean error (ME) of 0.019 Å and is the second most balanced functional between underestimation and overestimation. The greatest reductions of error by TM relative to TPSS were achieved for K, NaF, and NaCl. Among the 22 solids, the TM functional has the highest accuracy in predicting the lattice constants of main-group metals Li and Al, semiconductors GaP and GaAs, and transition metals Cu and Ag. Overall, TM is one of the most accurate functionals for lattice constants, with a mean absolute error (MAE) of 0.025 Å which is the smallest among all semilocal functionals listed, and on par with the MAE of PBEsol. (The SCAN functional [5] also yields very accurate lattice constants.) The MAE of the TM functional is larger than those of the nonlocal HSE06 (MAE = 0.013 Å) and optB86b-vdW (MAE = 0.017 Å) functionals. These nonlocal functionals outperform all the listed semilocal density functionals, but at a higher computational cost.

3.2 Bulk Moduli

Bulk modulus is related to the curvature of the total energy as a function of unit cell volume at the equilibrium geometry. This quantity can be calculated from various EOS models. [30–32] Bulk modulus presents a great challenge to DFT, in particular for transition metals. [33]

In the present work, to obtain the zero-temperature equilibrium lattice constant and bulk modulus for each crystal, calculations of the total energy were first performed on no less than 10 static lattices. The unit cells of such lattices have volumes ranging from -5% to +5% of the equilibrium cell volume. In order to make direct comparison with other functionals, in this work, we generate the equilibrium unit cell volume and bulk modulus by fitting energy versus unit cell volume to the stabilized jellium equation of state (SJEOS) [30,31]

$$\varepsilon(x) = \frac{a}{x^3} + \frac{b}{x^2} + \frac{c}{x} + d \ , \tag{7}$$

Table II: Equilibrium (0 K) lattice constants (Å) of 22 solids calculated with various functionals. The ME and MAE are in reference to experimental lattice constants. The LSDA, PBE, TPSS, PBEsol, and revTPSS values for Ge, BP, AlP, AlAs, GaN, GaP, and MgS are from Ref. 34. The other LSDA, PBE, and TPSS values are from Ref. 24, PBEsol from Ref. 35. The revTPSS results are taken from Ref. 36 except for potassium which is from Ref. 34. The HSE06 values are from Ref. 37. The optB86b-vdW value for BP is from Ref. 38. All other values of optB86b-vdW are from Ref. 39. The experimental data (in parentheses) and ZPE-corrected values (preceding the parentheses) for lattice constants are from Ref. 40. The TM values are calculated self-consistently. The smallest and largest MAEs for semilocal functionals are in bold blue and red, respectively.

Solids	Expt.	LSDA	PBE	PBEsol	TPSS	revTPSS	TM	HSE06	optB86b-vdW
Li	3.451 (3.477)	3.383	3.453	3.453	3.475	3.425	3.445	3.460	3.452
K	5.212 (5.225)	5.093	5.308	5.232	5.362	5.325	5.265		5.202
Al	4.019 (4.032)	4.008	4.063	4.038	4.035	4.005	4.024	4.022	4.036
C	3.544 (3.567)	3.544	3.583	3.562	3.583	3.559	3.564	3.549	3.572
Si	5.415 (5.430)	5.426	5.490	5.442	5.477	5.437	5.443	5.435	5.447
SiC	4.340 (4.358)	4.351	4.401	4.381	4.392	4.358	4.374	4.347	4.369
Ge	5.639 (5.652)	5.624	5.764	5.679	5.723	5.680	5.671	5.682	5.725
BP	4.520 (4.538)	4.491	4.548	4.520	4.544	4.529	4.534	4.519	4.545
AlP	5.445 (5.460)	5.433	5.504	5.468	5.492	5.482	5.487	5.472	
AlAs	5.646 (5.658)	5.631	5.728	5.676	5.702	5.682	5.691	5.687	
GaN	4.520 (4.531)	4.457	4.549	4.499	4.532	4.518	4.492	4.494	
GaP	5.435 (5.448)	5.392	5.506	5.439	5.488	5.460	5.437	5.462	
GaAs	5.637 (5.648)	5.592	5.726	5.687	5.702	5.673	5.641	5.687	5.717
NaCl	5.565 (5.595)	5.471	5.698	5.611	5.696	5.671	5.618	5.659	5.627
NaF	4.576 (4.609)	4.505	4.700	4.633	4.706	4.674	4.626	4.650	4.658
LiCl	5.072 (5.106)	4.968	5.148	5.072	5.113	5.087	5.089	5.115	5.103
LiF	3.960 (4.010)	3.904	4.062	4.002	4.026	4.011	3.995	4.018	4.037
MgO	4.186 (4.207)	4.156	4.242	4.229	4.224	4.233	4.209	4.210	4.230
MgS	5.182 (5.202)	5.127	5.228	5.184	5.228	5.222	5.198		
Cu	3.596 (3.603)	3.530	3.636	3.578	3.593	3.548	3.587	3.638	3.605
Pd	3.913 (3.916)	3.851	3.950	3.888	3.917	3.876	3.900	3.921	3.909
Ag	4.062 (4.069)	3.997	4.130	4.045	4.076	4.050	4.052	4.142	4.101
ME		-0.046	0.067	0.017	0.052	0.026	0.019	0.031	0.037
		(-0.064)	(0.049)	(-0.001)	(0.034)	(0.007)	(0.000)	(0.034)	(0.039)
MAE		0.048	**0.067**	**0.025**	0.053	0.039	**0.025**	0.013	0.017
		(0.064)	(0.051)	(0.019)	(0.035)	(0.029)	(0.017)	(0.024)	(0.024)

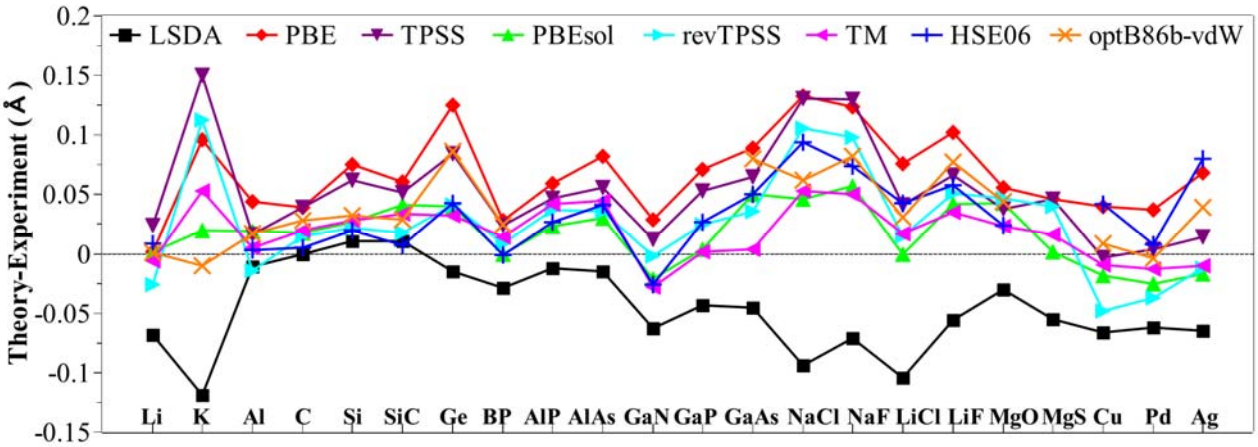

Figure 1 Performance of various density functionals for lattice constants of 22 solids. The references used are ZPE-corrected experimental values at 0 K. All values are from Table II.

where ε is the energy of the lattice cell, and x is the volume. The equilibrium lattice volume v_0 and bulk modulus B_0 were obtained by solving

$$a = \frac{9}{2} B_0 v_0 (B_1 - 3), \tag{8}$$

$$b = \frac{9}{2} B_0 v_0 (10 - 3B_1), \tag{9}$$

$$c = -\frac{9}{2} B_0 v_0 (11 - 3B_1). \tag{10}$$

Listed in Table III are the equilibrium bulk moduli of the 22 solids calculated with TM and other functionals. Figure 2 shows deviations of the LSDA, PBE, TPSS, PBEsol, TM, HSE06, and optB86b-vdW bulk moduli from the experimental data for these solids. The TM functional is less accurate than PBEsol and nonlocal functionals HSE06 and optB86b-vdW, but outperforms all-purpose functionals

Table III: Equilibrium bulk moduli (GPa) of the 22 solids calculated at 0 K. The LSDA, PBE, and TPSS values are from Ref. 24. The PBEsol values are from Ref. 41. For BP, AlP, AlAs, GaN, GaP, and MgS, the LSDA and PBE values are from Ref. 42 and the PBEsol values are from Ref. 43. The HSE06 values are from Ref. 43. The optB86b-vdW value for BP is from Ref. 38. All other values of optB86b-vdW are from Ref. 39. The experimental values of bulk moduli for the 22 solids are from the following references: Li, [44] K, [45] Al, [46] C [47], Si, [48] SiC, [49] Ge, [48] BP, [50] AlP, [51] AlAs, [51] GaN, [52] GaP, [51] GaAs, [48] NaCl, [53] NaF, [53] LiCl, [53] LiF, [54] MgO, [55] MgS, [56] Cu, [57] Pd, [58] and Ag. [59] The smallest and largest MAEs for semilocal functionals are in bold blue and red, respectively.

Solids	Expt.	LSDA	PBE	TPSS	PBEsol	TM	HSE06	optB86b-vdW
Li	13	14.7	13.7	13.2	13.8	13.7		13.4
K	3.7	4.6	3.8	3.6	3.7	4.0		3.79
Al	79.4	82.5	76.8	85.2	82.6	88.6		77.0
C	443	458	426	421	450.0	442.4	468.2	431
Si	99.2	95.6	89	91.9	94.2	97.1	99.6	91.2
SiC	225	225	209	213	218.0	220.0	233.3	215
Ge	75.8	75.9	63.0	66.4	68.1	72.5	73.5	61.5
BP	173	176	162		173.4	171.5	178.4	163.3
AlP	86	89.9	82.6		90.5	89.3	94.3	
AlAs	82	75.5	67.0		78.7	75.2	81.9	
GaN	190	204	173		182.8	207.1	193.0	
GaP	88	90.6	77.0		85.9	89.2	88.8	
GaAs	75.6	81.3	68.1	70.1	69.1	78.6	72.2	63.6
NaCl	26.6	32.5	23.9	23	25.8	26.9	25.9	26.2
NaF	51.4	63.3	47.7	44	48.6	52.5	54.5	47.5
LiCl	35.4	42	32.9	34.3	35.2	36.2	34.5	34.3
LiF	69.8	87.5	65.9	67.2	73.1	74.4	76.4	70.2
MgO	165	183	162	169	157.0	174.5	172.9	156
MgS	78.9	84.0	74.4		60.9	79.8	62.2	
Cu	142	192	153	173	166.0	180.2		149
Pd	195	240	180	203	205.0	210.7		187
Ag	109	153	107	129	119.0	138.4		104
ME		11.1	-6.8	-0.1	-0.2	5.3	2.8	-5.2
MAE		**12.0**	7.8	8.8	**6.0**	7.0	5.8	6.1
MARE		13.0	7.5	8.1	5.8	6.5	5.0	5.6

TPSS, PBE, as well as LSDA. Compared to lattice constants, the advantage of the two nonlocal functionals HSE06 and optB86b-vdW over the listed semilocal functionals has decreased significantly in the case of bulk moduli, suggesting relative insignificance of nonlocality for the curvature of the

potential energy curve. Nevertheless, nonlocality is still helpful in predicting bulk moduli, as can be seen from the error reduction from PBE to PBE-based range-separation functional HSE06.

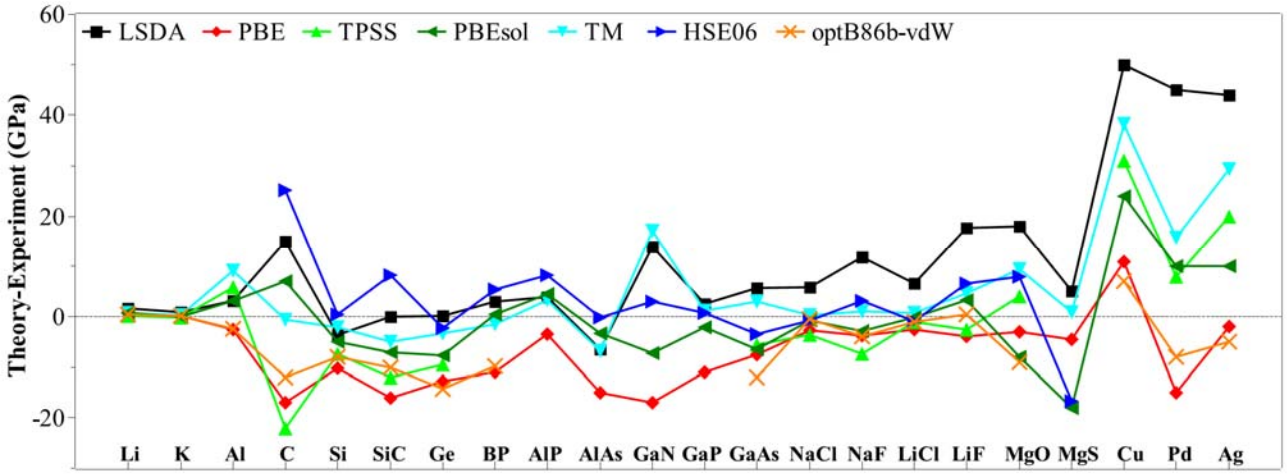

Figure 2 Performance of various density functionals for bulk moduli of 22 solids at 0 K. All values are from Table III.

3.3 Semiconductor Band Gaps

The electronic band gap is a key property of a semiconductor necessary for understanding its electrical, optical, photovoltaic, and photocatalytic properties.[60,61] We have assessed performance of the TM functional on 30 semiconductors. The TM results are listed in Table IV, along with other calculated values from the literature. All calculated band gaps reported in this work were obtained as the difference between the valence band maximum and conduction band minimum. From Table IV, we see that, like other density functionals, the TM functional tends to underestimate band gaps. The MAE of the TM functional is 0.87 eV, which is larger than that of TPSS (MAE = 0.79 eV) but 6~20% smaller than those of LSDA, PBE, PBEsol, and revTPSS. Compared to the nonlocal functional HSE06, the errors of

Table IV: Band gaps (in eV) of 30 semiconductors. The LSDA, PBE, PBEsol, TPSS, and revTPSS values are from Ref. 62. The HSE06 values are from Ref. 63. The experimental values are from Ref. 22. The smallest and largest MAEs for semilocal functionals are in bold blue and red, respectively.

Solid	Expt.	LSDA	PBE	PBEsol	TPSS	revTPSS	TM	HSE06
C	5.48	4.22	4.24	4.03	4.29	4.05	4.12	5.43
Si	1.17	0.62	0.72	0.53	0.80	0.63	0.56	1.21
Ge	0.74	0.00	0.13	0.00	0.32	0.14	0.35	0.80
SiC	2.42	1.42	1.46	1.27	1.42	1.23	1.24	2.32
BP	2.40	1.36	1.40	1.24	1.45	1.28	1.27	2.13
BAs	1.46	1.19	1.25	1.10	1.27	1.13	1.10	1.88
AlP	2.51	1.64	1.78	1.56	1.86	1.72	1.10	2.42
AlAs	2.23	1.43	1.55	1.37	1.66	1.57	1.47	2.13
AlSb	1.68	1.34	1.44	1.22	1.58	1.40	1.28	1.82
GaN	3.50	2.18	2.22	1.85	2.15	1.71	1.71	3.48
β-GaN	3.30	1.84	1.86	1.70	1.79	1.53	2.06	3.08
GaP	2.35	1.63	1.80	1.62	1.89	1.77	1.64	2.39
GaAs	1.52	0.04	0.36	0.42	0.60	0.73	0.68	1.11
GaSb	0.73	0.00	0.19	0.06	0.39	0.31	0.51	0.90
InN	0.69	0.00	0.00	0.00	0.00	0.01	0.00	0.72
InP	1.42	0.74	0.99	0.83	1.19	1.00	1.19	1.77
InAs	0.41	0.00	0.00	0.00	0.08	0.00	0.19	0.57
InSb	0.23	0.00	0.00	0.00	0.00	0.00	0.14	0.47
ZnS	3.66	2.02	2.30	2.22	2.53	2.42	2.40	3.44
ZnSe	2.70	1.05	1.37	1.26	1.62	1.58	1.61	2.38
ZnTe	2.38	1.11	1.39	1.29	1.65	1.60	1.70	2.34
CdS	2.55	0.97	1.26	1.08	1.47	1.31	1.33	2.21
CdSe	1.90	0.31	0.63	0.45	0.85	0.77	1.33	1.48
CdTe	1.92	0.54	0.81	0.67	1.05	0.98	1.10	1.64
MgS	5.40	3.37	3.65	3.34	3.91	2.68	3.76	4.67
MgSe	2.47	1.74	1.90	1.70	2.21	2.03	1.97	2.69
MgTe	3.60	2.41	2.65	2.58	3.07	3.08	2.98	3.54
BaS	3.88	2.13	2.40	2.15	2.56	2.48	2.34	3.19
BaSe	3.58	1.84	2.05	1.83	2.18	2.17	2.03	2.74
BaTe	3.08	1.48	1.66	1.38	1.77	1.69	1.61	2.21
ME		-1.09	-0.93	-1.09	-0.79	-0.95	-0.89	-0.14
MAE		**1.09**	0.93	**1.09**	**0.79**	0.95	0.89	0.26

semilocal functionals are too large, suggesting the significance of nonlocality [8] in band gap calculations.

A noteworthy feature of the TM functional is its greater ability to distinguish small-gap semiconductors from metals. Among the 30 semiconductors, InN is the only material which is qualitatively incorrectly predicted by the TM functional to have a zero band gap, while other semilocal density functionals predicts zero band gaps for multiple semiconductors: LSDA (5 semiconductors), PBE (3 semiconductors), PBEsol (4 semiconductors), TPSS (2 semiconductors), and revTPSS (2 semiconductors). The numerical values of the band gaps predicted by the TM functionals for such small-gap semiconductors are the most accurate among all semilocal functionals listed.

3.4 Cohesive Energies

Cohesive energy is the difference between the total electronic energy of a solid and the constituent neutral atoms. It is the condensed-matter analog of molecular atomization energy and a measure of the interatomic bond strength. To compute the cohesive energy for each of the 7 solids, the total energy of a unit cell was first divided by the number of atoms in the cell to get the total energy per atom. This energy per atom was then corrected by adding the phonon ZPE to account for the zero-point motion. The phonon ZPE per atom can be estimated from [30]

$$\varepsilon_{\mathrm{ZPE}} = \frac{9}{8} k_B \Theta_D , \tag{11}$$

where k_B is the Boltzmann constant and Θ_D is the Debye temperature of the solid. In the present work, we adopted the following Debye temperatures: C 2230K, [64] Si 645K, [64] SiC 1232K, [65] NaCl 321K, [64] NaF 492K, [64] LiCl 422K, [64] and LiF 732K. [64] The ZPE-corrected energy per atom was then subtracted from the spin-unrestricted ground-state energy of isolated atoms to obtain the cohesive energy. Among the 6 atoms (C, Si, Na, Li, Cl, F) comprising the 7 solids, the atoms Li and Na involve diffuse functions in their molecular basis sets. These diffuse basis functions were excluded from the calculations of lattice constants and bulk moduli of Li- and Na-containing ionic solids, but used for calculating the ground-state

Table V: Cohesive energies (eV/atom) of 7 solids. The LSDA, PBE, and TPSS values are from Ref. 24, PBEsol from Ref. 41, revTPSS from Ref. 66, HSE06 from Ref. 37, and optB86b-vdW from Ref. 39. The TM values are calculated self-consistently and corrected for zero-point vibrations. The smallest and largest MAEs for semilocal functionals are in bold blue and red, respectively.

Solid	Expt.	LSDA	PBE	TPSS	PBEsol	revTPSS	TM	HSE06	optB86b-vdW
C	7.37	8.83	7.62	7.12	8.05	7.31	7.48	7.43	7.66
Si	4.62	5.26	4.50	4.36	4.87	4.50	4.61	4.52	4.81
SiC	6.37	7.25	6.25	6.02	6.75	6.26	6.29	6.28	6.55
NaCl	3.31	3.58	3.16	3.18	3.20	3.14	3.19	3.06	3.29
NaF	3.93	4.50	3.96	3.87	3.99	3.74	3.88	3.67	3.95
LiCl	3.55	3.88	3.41	3.41	3.49	3.39	3.42	3.33	3.56
LiF	4.40	5.02	4.42	4.32	4.49	4.23	4.34	4.18	4.43
ME		0.68	-0.03	-0.18	0.18	-0.14	-0.05	-0.16	0.10
MAE		**0.68**	0.12	0.18	0.23	0.14	**0.08**	0.17	0.11
MARE		13.4	2.5	3.7	4.2	3.4	1.9	4.3	1.9

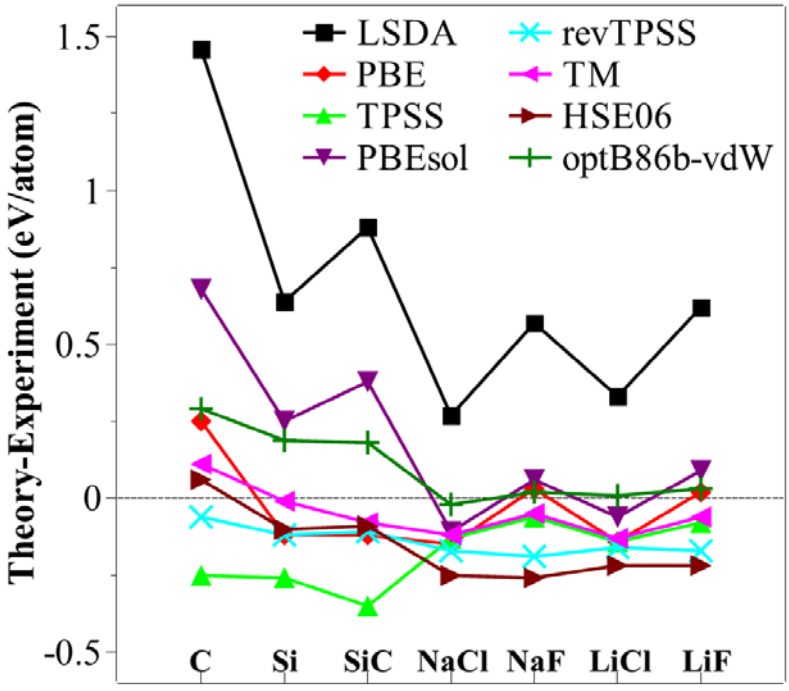

Figure 3 Performance of various density functionals for cohesive energies of 7 solids. All values are from Table V.

energies of the isolated Li and Na atoms (i.e., the full molecular basis set 6-311G* was employed for the isolated Li and Na atoms). Applying different basis sets to the solid and the corresponding isolated atoms provides reasonable cohesive energies for ionic solids, because cations are compact and their electrons are less likely to appear in the far regions described by diffuse functions, therefore decreasing the need of diffuse functions in the solid-state calculation. Listed in Table V are the cohesive energies of 7 solids. Figure 3 compares the performance of the LSDA, PBE, TPSS, PBEsol, revTPSS, TM, HSE06, and optB86b-vdW functionals for cohesive energies of these 7 solids. Overall, TM has an MAE of only 0.08 eV/atom, with an error reduction of over 50% from that of the meta-GGA TPSS. The TM functional is also significantly more accurate than the other semilocal functionals revTPSS, PBE, PBEsol, and LSDA. This is in sharp contrast with atomization energies of molecular systems,[10] for which TM is less accurate than TPSS for the 148 G2 molecules and moderately more accurate than TPSS for the AE6 test set. The TM functional can even provide better description of cohesive energies than the nonlocal functionals HSE06 and optB86b-vdW.

3.5 Surface Exchange and Correlation Energies

Jellium, a homogeneous electron gas with a positive uniform background charge, is a realistic model of simple metals. The electron density of jellium is uniform within the bulk, while near the surface it varies rapidly and decays exponentially in vacuum. The surface energy σ is defined as the energy per unit area needed to cut the bulk jellium into two infinitely separate parts. The exchange-correlation contribution to the surface energy can be calculated as

$$\sigma_{\mathrm{xc}} = \int_{-\infty}^{\infty} n(z)[\epsilon_{\mathrm{xc}}(z) - \epsilon_{\mathrm{xc}}(-\infty)]dz. \tag{12}$$

From this equation, we can see that, in order to have an accurate description of the surface energy, a density functional must be correct for slowly varying densities. This is true even for real solids,[67] because the typical valence electron density of solids is slowly varying.

Several *ab initio* calculations of the jellium surface energy are available in the literature, including the random-phase approximation (RPA)[68] and quantum Monte Carlo (QMC)[69]. These calculations agree well with each other and with time-dependent DFT.[68] Since QMC values have some uncertainty, we compare all DFT values to the RPA calculation in the high-density regime from r_s = 2 bohrs to r_s = 3 bohrs, in which the RPA is reliable. The results displayed in Table VI show that the surface exchange energy from the TM exchange functional is in excellent agreement with the exact values,[70] better than the LSDA, PBE, and TPSS values. Specifically, the TM functional has an MAE of only 10 erg/cm^2, an overwhelming 80~96% decrease of error compared with LSDA, PBE, and TPSS. This excellent performance of the TM functional largely benefits from the recovery of the correct fourth-order gradient expansion in the slowly varying limit. As a result, TM yields much better surface exchange-correlation energy than LSDA, PBE, and TPSS.

Table VI: Jellium surface exchange energies σ_x and surface exchange-correlation energies σ_{xc} (in erg/cm^2). The reference values are taken from the RPA calculation.[70] The LSDA, PBE, and TPSS values are taken from Ref. 24. The smallest and largest MAEs are in bold blue and red, respectively.

	Exchange					Exchange-correlation				
r_s (bohr)	LSDA	PBE	TPSS	TM	RPA	LSDA	PBE	TPSS	TM	RPA
2.00	3037	2438	2553	2641	2624	3354	3265	3380	3515	3467
2.07	2674	2127	2231	2312	2296	2961	2881	2985	3109	3064
2.30	1809	1395	1469	1531	1521	2019	1962	2035	2132	2098
2.66	1051	770	817	860	854	1188	1152	1198	1267	1240
3.00	669	468	497	528	526	764	743	772	823	801
ME	284	-125	-51	10		-77	-133	-60	35	
MAE	**284**	125	51	**10**		77	**133**	60	**35**	

4. CONCLUSIONS

In summary, we have evaluated the performance of the TM meta-GGA on solids and solid surfaces for a number of properties including lattice constants, bulk moduli, band gaps, cohesive energies, and jellium surface exchange-correlation energies. Our calculations show that this functional is consistently accurate for the properties considered. In particular, the TM functional is the most accurate semilocal density functional among those considered for both the lattice constants and cohesive energies, indicating its great potential utility in computational studies of the structure and energetics of solids. The TM functional also achieves excellent accuracy for jellium surface exchange-correlation energies. However, like all other semilocal functionals, the TM functional tends to underestimate band gaps, because it misses the functional derivative discontinuity [71] required for accurate band gap prediction. Nevertheless, the TM functional demonstrates very strong capability of distinguishing small-gap semiconductors from metals, as it predicts a zero band gap for only one of the 30 test semiconductors, which is the best result among all semilocal functionals considered.

The performance of the TM functional greatly benefits from (i) recovery of the correct slowly-varying gradient expansion, the paradigm of condensed-matter physics, and (ii) slow increase of the enhancement factor with density gradient. The first property is very important for surface energy calculations, while the second is helpful in capturing the van der Waals interactions, [72–79] as demonstrated by the excellent performance of the TM functional for lattice constants (Table II) and cohesive energies (Table V). Recently, we have also assessed [80] the TM functional on diverse molecular properties and found that it has a similarly good accuracy for atoms and molecules as for solids. The balanced description of finite and extended systems by the TM functional makes it an attractive tool for studying new materials whose properties are yet unknown.

Acknowledgments

We thank Professor Guocai Tian for many helpful discussions and valuable suggestions. YM and JT acknowledge support from NSF under Grant no. CHE-1640584. JT also acknowledges support from Temple University via John Perdew. VNS was supported by the Natural Sciences and Engineering Research Council of Canada (NSERC). GES was supported by the U.S. Department of Energy, Office of Basic Energy Sciences, Computational and Theoretical Chemistry Program under Award No. DE-FG02-09ER16053. GES is a Welch Foundation Chair (C-0036). Computational support was provided by Temple University.

* Corresponding author. jianmin.tao@temple.edu

References:

[1] W. Kohn and L. J. Sham, Phys. Rev. **140**, A1133 (1965).
[2] J. P. Perdew, K. Burke, and M. Ernzerhof, Phys. Rev. Lett. **77**, 3865 (1996).
[3] J. Tao, J. P. Perdew, V. N. Staroverov, and G. E. Scuseria, Phys. Rev. Lett. **91**, 146401 (2003).
[4] Y. Zhao and D. G. Truhlar, Theor. Chem. Acc. **120**, 215 (2008).
[5] J. Sun, A. Ruzsinszky, and J. P. Perdew, Phys. Rev. Lett. **115**, 036402 (2015).
[6] L. A. Constantin, J. P. Perdew, and J. Tao, Phys. Rev. B **73**, 205104 (2006).
[7] L. A. Constantin, E. Fabiano, and F. Della Sala, Phys. Rev. B **88**, 125112 (2013).
[8] J. Tao, I. W. Bulik, and G. E. Scuseria, https://arxiv.org/abs/1609.04839.
[9] A. D. Becke and M. R. Roussel, Phys. Rev. A **39**, 3761 (1989).
[10] J. Tao and Y. Mo, Phys. Rev. Lett. **117**, 073001 (2016).
[11] J. W. Negele and D. Vautherin, Phys Rev C **5**, 1472 (1972).
[12] P. S. Svendsen and U. von Barth, Phys. Rev. B **54**, 17402 (1996).
[13] M. Levy, Phys. Rev. A **43**, 4637 (1991).
[14] Y. Fang, B. Xiao, J. Tao, J. Sun, and J. P. Perdew, Phys. Rev. B **87**, 214101 (2013).
[15] F. Tran, J. Stelzl, and P. Blaha, J. Chem. Phys. **144**, 204120 (2016).
[16] J. Tao, F. Zheng, J. P. Perdew, and A. M. Rappe, submitted.
[17] M. J. Frisch *et al*, *Gaussian 09, Revision A.02* (Gaussian, Inc., Wallingford CT, 2009).
[18] K. N. Kudin and G. E. Scuseria, Phys. Rev. B **61**, 16440 (2000).
[19] K. Doll, N. M. Harrison, and V. R. Saunders, J. Phys. Condens. Matter **11**, 5007 (1999).
[20] J. E. Jaffe, Z. Lin, and A. C. Hess, Phys. Rev. B **57**, 11834 (1998).
[21] J. C. Boettger, U. Birkenheuer, S. Krüger, N. Rösch, and S. B. Trickey, Phys. Rev. B **52**, 2025 (1995).
[22] J. Heyd, J. E. Peralta, G. E. Scuseria, and R. L. Martin, J. Chem. Phys. **123**, 174101 (2005).

[23] R. Pandey, J. E. Jaffe, and N. M. Harrison, J. Phys. Chem. Solids **55**, 1357 (1994).
[24] V. N. Staroverov, G. E. Scuseria, J. Tao, and J. P. Perdew, Phys. Rev. B **69**, 075102 (2004).
[25] M. Catti, G. Valerio, R. Dovesi, and M. Causà, Phys. Rev. B **49**, 14179 (1994).
[26] K. Doll and N. M. Harrison, Chem. Phys. Lett. **317**, 282 (2000).
[27] P. J. Hay and W. R. Wadt, J. Chem. Phys. **82**, 299 (1985).
[28] Pd_HAYWSC-2111d31 basis: http://www.crystal.unito.it/Basis_Sets/palladium.html
[29] Ag_HAYWSC-2111d31G basis: http://www.crystal.unito.it/Basis_Sets/silver.html
[30] A. B. Alchagirov, J. P. Perdew, J. C. Boettger, R. C. Albers, and C. Fiolhais, Phys. Rev. B **63**, 224115 (2001).
[31] A. B. Alchagirov, J. P. Perdew, J. C. Boettger, R. C. Albers, and C. Fiolhais, Phys. Rev. B **67**, 026103 (2003).
[32] F. Birch, Phys. Rev. **71**, 809 (1947).
[33] P. Janthon, S. (Andy) Luo, S. M. Kozlov, F. Viñes, J. Limtrakul, D. G. Truhlar, and F. Illas, J. Chem. Theory Comput. **10**, 3832 (2014).
[34] P. Hao, Y. Fang, J. Sun, G. I. Csonka, P. H. T. Philipsen, and J. P. Perdew, Phys. Rev. B **85**, 014111 (2012).
[35] J. P. Perdew, A. Ruzsinszky, G. I. Csonka, O. A. Vydrov, G. E. Scuseria, L. A. Constantin, X. Zhou, and K. Burke, Phys. Rev. Lett. **100**, 136406 (2008).
[36] J. P. Perdew, A. Ruzsinszky, G. I. Csonka, L. A. Constantin, and J. Sun, Phys. Rev. Lett. **103**, 026403 (2009).
[37] L. Schimka, J. Harl, and G. Kresse, J. Chem. Phys. **134**, 024116 (2011).
[38] L. Shulenburger and T. R. Mattsson, Phys. Rev. B **88**, 245117 (2013).
[39] J. Klimeš, D. R. Bowler, and A. Michaelides, Phys. Rev. B **83**, 195131 (2011).
[40] P. Haas, F. Tran, and P. Blaha, Phys. Rev. B **79**, 085104 (2009).
[41] G. I. Csonka, J. P. Perdew, A. Ruzsinszky, P. H. T. Philipsen, S. Lebègue, J. Paier, O. A. Vydrov, and J. G. Ángyán, Phys. Rev. B **79**, 155107 (2009).
[42] F. Tran, R. Laskowski, P. Blaha, and K. Schwarz, Phys. Rev. B **75**, 115131 (2007).
[43] P. Pernot, B. Civalleri, D. Presti, and A. Savin, J. Phys. Chem. A **119**, 5288 (2015).
[44] R. A. Felice, J. Trivisonno, and D. E. Schuele, Phys. Rev. B **16**, 5173 (1977).
[45] W. R. Marquardt and J. Trivisonno, J. Phys. Chem. Solids **26**, 273 (1965).
[46] G. N. Kamm and G. A. Alers, J. Appl. Phys. **35**, 327 (1964).
[47] M. Levinshtein, S. Rumyantsev, and M. Shur, *Handbook Series on Semiconductor Parameters* (World Scientific, Singapore, 1996).
[48] K.-H. Hellwege, *Landolt–Bornstein, New Series, Group III* (Springer, Berlin, 1966).
[49] W. R. L. Lambrecht, B. Segall, M. Methfessel, and M. van Schilfgaarde, Phys. Rev. B **44**, 3685 (1991).
[50] S. Kalvoda, B. Paulus, P. Fulde, and H. Stoll, Phys. Rev. B **55**, 4027 (1997).
[51] D. Bimberg *et al*, *Semiconductors. Physics of Group IV Elements and III-V Compounds.* (Springer-Verlag GmbH, 1982).
[52] H. M. Tütüncü, S. Bağci, G. P. Srivastava, A. T. Albudak, and G. Uğur, Phys. Rev. B **71**, 195309 (2005).
[53] J. T. Lewis, A. Lehoczky, and C. V. Briscoe, Phys. Rev. **161**, 877 (1967).
[54] C. V. Briscoe and C. F. Squire, Phys. Rev. **106**, 1175 (1957).
[55] K. Marklund and S. A. Mahmoud, Phys. Scr. **3**, 75 (1971).
[56] S. M. Peiris, A. J. Campbell, and D. L. Heinz, J. Phys. Chem. Solids **55**, 413 (1994).
[57] W. C. Overton and J. Gaffney, Phys. Rev. **98**, 969 (1955).

[58] D. K. Hsu and R. G. Leisure, Phys. Rev. B **20**, 1339 (1979).
[59] J. R. Neighbours and G. A. Alers, Phys. Rev. **111**, 707 (1958).
[60] N. López, L. A. Reichertz, K. M. Yu, K. Campman, and W. Walukiewicz, Phys. Rev. Lett. **106**, 028701 (2011).
[61] X. Chen, L. Liu, P. Y. Yu, and S. S. Mao, Science **331**, 746 (2011).
[62] R. Peverati and D. G. Truhlar, J. Chem. Phys. **136**, 134704 (2012).
[63] A. J. Garza and G. E. Scuseria, J. Phys. Chem. Lett. **7**, 4165 (2016).
[64] D. E. Gray, *American Institute of Physics Handbook* (McGraw–Hill, New York, 1972).
[65] A. Zywietz, K. Karch, and F. Bechstedt, Phys. Rev. B **54**, 1791 (1996).
[66] J. Sun, M. Marsman, G. I. Csonka, A. Ruzsinszky, P. Hao, Y.-S. Kim, G. Kresse, and J. P. Perdew, Phys. Rev. B **84**, 035117 (2011).
[67] P. Lazar and M. Otyepka, Phys. Rev. B **91**, 115402 (2015).
[68] L. A. Constantin, J. M. Pitarke, J. F. Dobson, A. Garcia-Lekue, and J. P. Perdew, Phys. Rev. Lett. **100**, 036401 (2008).
[69] B. Wood, N. D. M. Hine, W. M. C. Foulkes, and P. García-González, Phys. Rev. B **76**, 035403 (2007).
[70] J. M. Pitarke and A. G. Eguiluz, Phys. Rev. B **63**, 045116 (2001).
[71] J. P. Perdew, R. G. Parr, M. Levy, and J. L. Balduz, Phys. Rev. Lett. **49**, 1691 (1982).
[72] B. Santra, J. Klimeš, D. Alfè, A. Tkatchenko, B. Slater, A. Michaelides, R. Car, and M. Scheffler, Phys. Rev. Lett. **107**, 185701 (2011).
[73] J. Tao, J. P. Perdew, and A. Ruzsinszky, Int. J. Mod. Phys. B **27**, 1330011 (2013).
[74] P. Hao, J. Sun, B. Xiao, A. Ruzsinszky, G. I. Csonka, J. Tao, S. Glindmeyer, and J. P. Perdew, J. Chem. Theory Comput. **9**, 355 (2013).
[75] J. Tao, J. Yang, and A. M. Rappe, J. Chem. Phys. **142**, 164302 (2015).
[76] J. G. Brandenburg and S. Grimme, in *Prediction and Calculation of Crystal Structures*, edited by S. Atahan-Evrenk and A. Aspuru-Guzik (Springer International Publishing, Cham, 2014).
[77] A. Otero-de-la-Roza and E. R. Johnson, J. Chem. Theory Comput. **11**, 4033 (2015).
[78] J. Tao and A.M. Rappe, J. Chem. Phys. (Communication) **144**, 031102 (2016).
[79] J. Tao, Y. Mo, G. Tian, and A. Ruzsinszky, Phys. Rev. B **94**, 085126 (2016).
[80] Y. Mo, G. Tian, R. Car, V. N. Staroverov, G. E. Scuseria, and J. Tao, J. Chem. Phys. (in press). http://arxiv.org/abs/1607.05249